

## [18] Identification and Characterization of Metal Ion Binding Sites in RNA

By RUBEN L. GONZALEZ, JR. and IGNACIO TINOCO, JR.

### Introduction

Metal ions are an integral component of RNA molecules. The highly complex tertiary structures adopted by large, biologically active RNA molecules necessarily involve the close packing of negatively charged backbone phosphate groups. This leads to formation of negatively charged, geometrically unique pockets ideal for the binding of positively charged metal ion complexes. Nuclear magnetic resonance (NMR) methods for studying the interaction of metal ions with RNA in solution have been available for some time. However, until recently, the structural characterization of metal ion binding sites in RNA has been restricted to crystallographic studies of RNA.<sup>1-4</sup> More recently, structural and thermodynamic studies of metal ion binding sites in RNA using solution state NMR have appeared. Here we review currently utilized NMR methods to study metal ion binding to RNA; we emphasize  $\text{Mg}(\text{H}_2\text{O})_6^{2+}$  metal ion binding sites characterized by intermolecular NOEs from  $\text{Co}(\text{NH}_3)_6^{3+}$  protons to RNA protons. These studies include an RNA molecule with tandem imino hydrogen bonded G·A mismatches as well as a GAAA tetraloop<sup>5</sup> derived from the P5 junction region of the *Tetrahymena thermophila* group I intron (Fig. 1A); two RNA molecules containing different arrangements of tandem G·U wobble base pairs<sup>6,7</sup> derived from the P5b and P5 helices of the *T. thermophila* group I intron (Figs. 1B and 1C); and the VPK viral RNA pseudoknot involved in -1 frameshifting in mouse mammary tumor virus (Fig. 2).<sup>8</sup> NMR methods that have been successfully applied to metal ion binding in proteins and could be effectively applied to RNA-metal ion studies are also discussed.

### Sample Preparation

One of the most important steps in a successful NMR study is sample preparation. RNA samples for metal ion studies are prepared as previously described,<sup>5-8</sup>

<sup>1</sup> S. R. Holbrook, J. L. Sussman, R. W. Warrant, G. M. Church, and S. H. Kim, *Nucl. Acids Res.* **8**, 2811 (1971).

<sup>2</sup> W. G. Scott, J. T. Finch, and A. Klug, *Cell* **81**, 991 (1995).

<sup>3</sup> J. H. Cate and J. A. Doudna, *Structure* **4**, 1221 (1996).

<sup>4</sup> C. C. Correl, B. Freeborn, P. B. Moore, and T. A. Steitz, *Cell* **91**, 705 (1997).

<sup>5</sup> S. Rüdiger and I. Tinoco, Jr., *J. Mol. Biol.* **295**, 1211 (2000).

<sup>6</sup> J. S. Kieft and I. Tinoco, Jr., *Structure* **5**, 713 (1997).

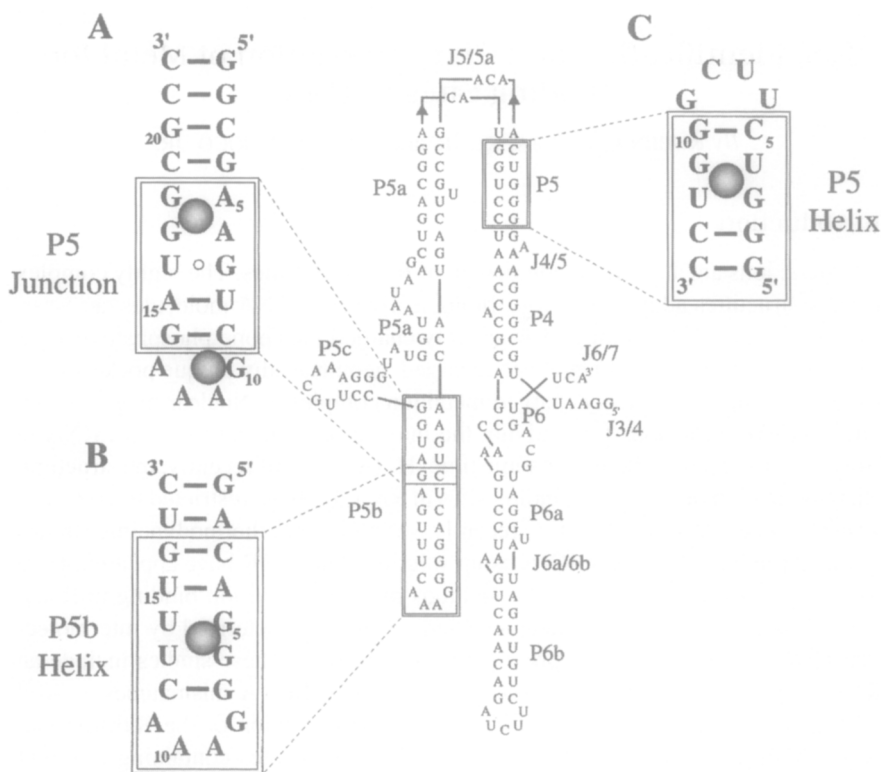


FIG. 1. Divalent metal ion binding sites characterized by NMR studies and derived from the P5 junction (A), P5b helix (B), and P5 helix (C) regions of the *Tetrahymena thermophila* group I intron P4-P6 domain. These sites include tandem imino-hydrogen bonded G · A mismatched base pairs (A), a GAAA tetraloop (A), and two sets of tandem G · U wobble base pairs (B) and (C). The gray spheres indicate the approximate positions of the metal ion in each binding site. The detailed structures of the binding sites at the two sets of tandem G · U base pairs and at the GAAA tetraloop were solved using intermolecular NOEs from the protons of  $\text{Co}(\text{NH}_3)_6^{3+}$  to RNA protons. In the P5b helix binding site (B), the metal ion binds in the major groove of the helix adjacent to the guanines in the G · U base pairs (G5 and G6) and forms hydrogen bonds with the N7 and O6 of these guanines. The metal ion in the P5 helix (C) also binds in the major groove at the center of the two G · U base pairs and can form hydrogen bonds with the O6 and N7 of the guanines in the G · U base pairs (G3 and G11) and the guanines in the G · C base pairs above and below the G · U base pairs (G2 and G10), as well as the O4 of the uracils in the G · U base pairs (U4 and U12). Both structures are in excellent agreement with metal ion binding sites observed in the P4-P6 crystal structure (see Ref. 3). The metal ion at the GAAA tetraloop had not been previously observed in crystal structures and binds in the major groove with electrostatic and hydrogen bonding interactions with the nonbridging phosphate oxygens of A12 and the N7 of G10. The binding site at the tandem G · A base pairs was identified using chemical shift changes and paramagnetic line broadening, but no intermolecular NOEs were observed and therefore the detailed structure of the binding site could not be solved.

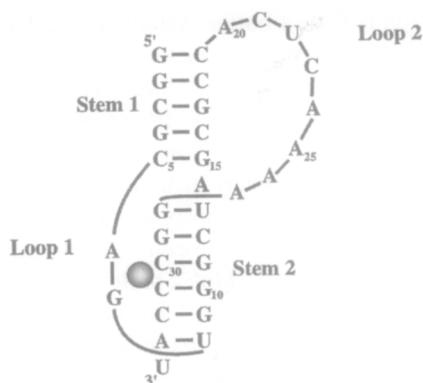


FIG. 2. Divalent metal ion binding site in the VPK mRNA pseudoknot derived from the  $-1$  frameshifter pseudoknot in mouse mammary tumor virus. The gray sphere indicates the approximate position of the metal ion in the binding site. The detailed structure of the metal ion binding site was solved using intermolecular NOEs from the  $\text{Co}(\text{NH}_3)_6^{3+}$  amino protons to RNA protons. The metal ion binds in the major groove of stem 2 stabilizing the tight turn between G7 and U8 and mediating the close packing of the two nucleotides of loop 1 against the major groove of stem 2. Within the family of structures, hydrogen bonds are possible to backbone nonbridging phosphate oxygens, sugar 2'-hydroxyl oxygens, and base nitrogens and oxygens in loop 1 and stem 2.

with the following special considerations. RNA concentrations<sup>7</sup> are generally  $500 \mu\text{M}$  for one-dimensional titration experiments and  $2 \text{ mM}$  for structural studies by two-dimensional NMR experiments. Volumes for NMR samples are typically  $400 \mu\text{l}$  in  $5 \text{ mm}$  Aldrich NMR tubes or  $250 \mu\text{l}$  in  $5 \text{ mm}$  Shigemi tubes. After *in vitro* transcription and purification,<sup>9,10</sup> RNA pellets are dissolved in a  $5 \text{ mM}$  EDTA solution. In order to remove trace metal ions, the RNA solution is dialyzed for 24 hr at  $4^\circ$  against  $5 \text{ mM}$  EDTA followed by dialysis at  $4^\circ$  against a  $10 \text{ mM}$  sodium phosphate (pH 6.4),  $200 \text{ mM}$  NaCl buffer solution. Using relatively high concentrations of sodium ion for the NMR experiments saturates the negatively charged phosphate backbone and minimizes nonspecific electrostatic interaction between the phosphate backbone and the metal ion complex under investigation. In some cases  $100 \mu\text{M}$  EDTA will be added to the final dialysis buffer to chelate any trace divalent metal ion contaminants not removed by dialysis. Because of the generally low-affinity binding of divalent metal ions to RNA, large concentrations of divalent metal ions are used in these studies and this trace amount of EDTA contributes insignificantly to the free metal ion concentration.

<sup>7</sup> G. Colmenarejo and I. Tinoco, Jr., *J. Mol. Biol.* **290**, 119 (1999).

<sup>8</sup> R. L. Gonzalez, Jr. and I. Tinoco, Jr., *J. Mol. Biol.* **289**, 1267 (1999).

<sup>9</sup> J. F. Milligan, D. R. Groebe, G. M. Witherall, and O. C. Uhlenbeck, *Nucl. Acids Res.* **15**, 8783 (1987).

<sup>10</sup> J. R. Wyatt, M. Chastain, and J. D. Puglisi, *Biotechniques* **11**, 764 (1991).

A final consideration is that of buffer system choice. Organic buffer systems that do not interact significantly with the metal ions can be used. However, if not deuterated, these buffers will produce very large  $^1\text{H}$  NMR resonances. A phosphate buffer system will not produce  $^1\text{H}$  NMR signals, but has the disadvantage that phosphate anions interact with metal ions and affect the free metal ion concentration. In the pH range used in many metal ion binding studies (pH 6–7), the dominant phosphate species present in phosphate buffer is  $\text{H}_2\text{PO}_4^-$ .<sup>11–13</sup> Binding of divalent metal ions to  $\text{H}_2\text{PO}_4^-$  has not been studied in detail, but equilibrium dissociation constants for  $\text{Mg}^{2+}$ ,  $\text{Ca}^{2+}$ ,  $\text{Mn}^{2+}$ , or  $\text{Sr}^{2+}$  bound to  $\text{HPO}_4^{2-}$  have been reported and are in the range of 2.5–30 mM.<sup>14</sup> The binding of metal ions to  $\text{H}_2\text{PO}_4^-$  is expected to be even weaker because of its reduced negative charge. However, the binding of metal ions to components of the buffer will affect binding constants to RNA. If the concentration of metal ion is established by equilibrium dialysis, the free ion concentration (the ion concentration in equilibrium with the RNA solution) includes that bound to buffer components. The apparent binding constant to the RNA will thus depend on the buffer used. Even if there is no metal ion binding to the buffer anions, the binding constants to the RNA will depend on the concentrations and identity of the added cations, because of competition for the metal ion binding sites on the RNA molecule.

### Diamagnetic Metal Ion Probes

Addition of a diamagnetic metal ion complex such as  $\text{Mg}^{2+}$  or  $\text{Co}(\text{NH}_3)_6^{3+}$  to an RNA molecule can lead to changes in NMR spectral features of RNA nuclei near the metal ion binding site and can therefore serve as probes for binding site identification (Fig. 3).<sup>5–8,15–19</sup> Typically the RNA sample is titrated with the diamagnetic metal ion and one-dimensional experiments are recorded in either 90%  $\text{H}_2\text{O}/10\%$   $\text{D}_2\text{O}$  or 99.9%  $\text{D}_2\text{O}$  solution. The chemical shifts and/or resonance line widths for well-resolved RNA resonances can then be recorded as a function of metal ion concentration. The imino proton region of the RNA NMR spectrum is usually well resolved and provides information about metal ions binding near base pairs regardless of whether binding takes place in the major or minor groove.

<sup>11</sup> R. G. Bates, *J. Res. Natl. Bur. Standards* **47**, 127 (1951).

<sup>12</sup> R. G. Bates and S. F. Acree, *J. Res. Natl. Bur. Standards* **30**, 129 (1943).

<sup>13</sup> J. J. Christensen, R. M. Izatt, L. D. Hansen, and J. A. Partridge, *J. Phys. Chem.* **70**, 2003 (1966).

<sup>14</sup> R. M. Smith and R. A. Alberty, *J. Am. Chem. Soc.* **78**, 2376 (1956).

<sup>15</sup> S. Limmer, H.-P. Hoffman, G. Ott, and M. Sprinzl, *PNAS* **90**, 6199 (1993).

<sup>16</sup> K. Kalurachchi and E. P. Nikonowicz, *J. Mol. Biol.* **280**, 639 (1999).

<sup>17</sup> P. L. Nixon, C. A. Theimer, and D. P. Giedroc, *Biopolymers* **50**, 443 (1999).

<sup>18</sup> M. R. Hansen, J. P. Simorre, P. Hanson, V. Mokler, L. Bellont, L. Beigelman, and A. Pardi, *RNA* **5**, 1099 (1999).

<sup>19</sup> S. E. Butcher, F. H.-T. Allain, and J. Feigon, *Biochemistry* **39**, 2174 (2000).

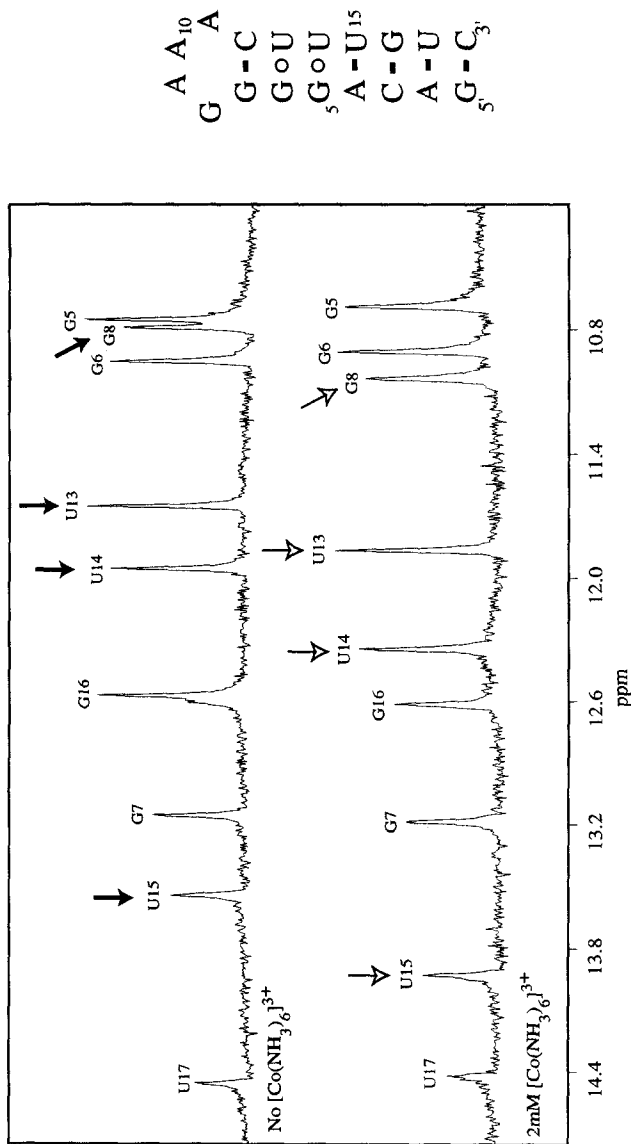


FIG. 3. Imino proton portion of a one-dimensional NMR spectrum of the P5b stem loop from the *T. thermophila* group I intron. Resonances corresponding to the U13, U14, U15, and G8 imino protons, denoted by arrows, shift downfield with no significant change in intensity and/or line width on addition of cobalt(III) hexammine. This is consistent with a fast exchange process on the chemical shift time scale. Similar trends are observed on the addition of  $Mg^{2+}$  ion. [Reprinted with permission from J. S. Kieft and J. Tinoco, Jr., *Structure* 5, 713 (1997)].

For these reasons this region of the spectrum provides a very good place to begin spectral analysis.

Generally, chemical shift and resonance line-width changes observed during diamagnetic metal ion titrations will be small. Spectral changes will depend on (i) direct changes in the magnetic environment of the observed nucleus caused by the bound ion, (ii) indirect effects caused by RNA conformational changes upon metal ion binding, and (iii) the exchange regime of the observed resonance on the time scale of the appropriate NMR parameter (e.g., chemical shift, scalar coupling, relaxation rate). In order to identify a binding site one would ideally prefer to separate the direct effect of the metal ion from effects due to conformational changes. Detection of intermolecular nuclear Overhauser effect (NOE) cross peaks between protons from a metal ion complex and protons from an RNA molecule or the use of paramagnetic metal ion probes provide methods of separating these two effects.

### *Intermolecular Nuclear Overhauser Effects*

Intermolecular nuclear Overhauser effect (NOE) cross peaks between protons from a metal ion complex and protons from an RNA molecule provide distance constraints that can be used to determine the structure of the metal ion binding site. Generally the native metal ion complexes that interact with RNA possess H<sub>2</sub>O ligands, which are unfavorable for the detection of intermolecular NOEs due to fast exchange with the bulk solvent water. Metal ion complexes with ligands other than water that are in slow exchange with the solvent can be used to mimic the native metal ion complex. Co(NH<sub>3</sub>)<sub>6</sub><sup>3+</sup> has been successfully used as a model for Mg(H<sub>2</sub>O)<sub>6</sub><sup>2+</sup> to solve the structures of several Mg(H<sub>2</sub>O)<sub>6</sub><sup>2+</sup> binding sites (Fig. 4).<sup>5-8</sup> Co(NH<sub>3</sub>)<sub>6</sub><sup>3+</sup> has been proposed as a substitute for Mg(H<sub>2</sub>O)<sub>6</sub><sup>2+</sup> based on geometric similarities.<sup>20</sup>

Intermolecular NOEs from Co(NH<sub>3</sub>)<sub>6</sub><sup>3+</sup> protons to RNA protons can be observed in a conventional H<sub>2</sub>O NOESY experiment (Figs. 4C and 4D). In a typical experiment,<sup>6</sup> a 2 mM RNA sample in 10 mM sodium phosphate (pH 6.4), 200 mM NaCl, 100 μM EDTA, and 2 mM Co(NH<sub>3</sub>)<sub>6</sub><sup>3+</sup> in 90% H<sub>2</sub>O/10% D<sub>2</sub>O is utilized. An H<sub>2</sub>O NOESY experiment is performed using the jump-return<sup>21</sup> water suppression scheme. Usually, the *t*<sub>2</sub> dimension will contain a very strong resonance for the Co(NH<sub>3</sub>)<sub>6</sub><sup>3+</sup> protons, and it will be difficult to detect the intermolecular NOEs. Intermolecular NOEs, however, are observable in the *t*<sub>1</sub> dimension at the Co(NH<sub>3</sub>)<sub>6</sub><sup>3+</sup> proton chemical shift of 3.65 ppm. Imino, amino, and aromatic proton to Co(NH<sub>3</sub>)<sub>6</sub><sup>3+</sup> proton cross peaks will be easily detected. Intermolecular cross peaks to the sugar protons and the H5 pyrimidine protons will be more difficult

<sup>20</sup> J. A. Cowan, *J. Inorg. Biochem.* **49**, 171 (1993).

<sup>21</sup> P. Plateau and M. Guéron, *J. Am. Chem. Soc.* **104**, 7310 (1982).

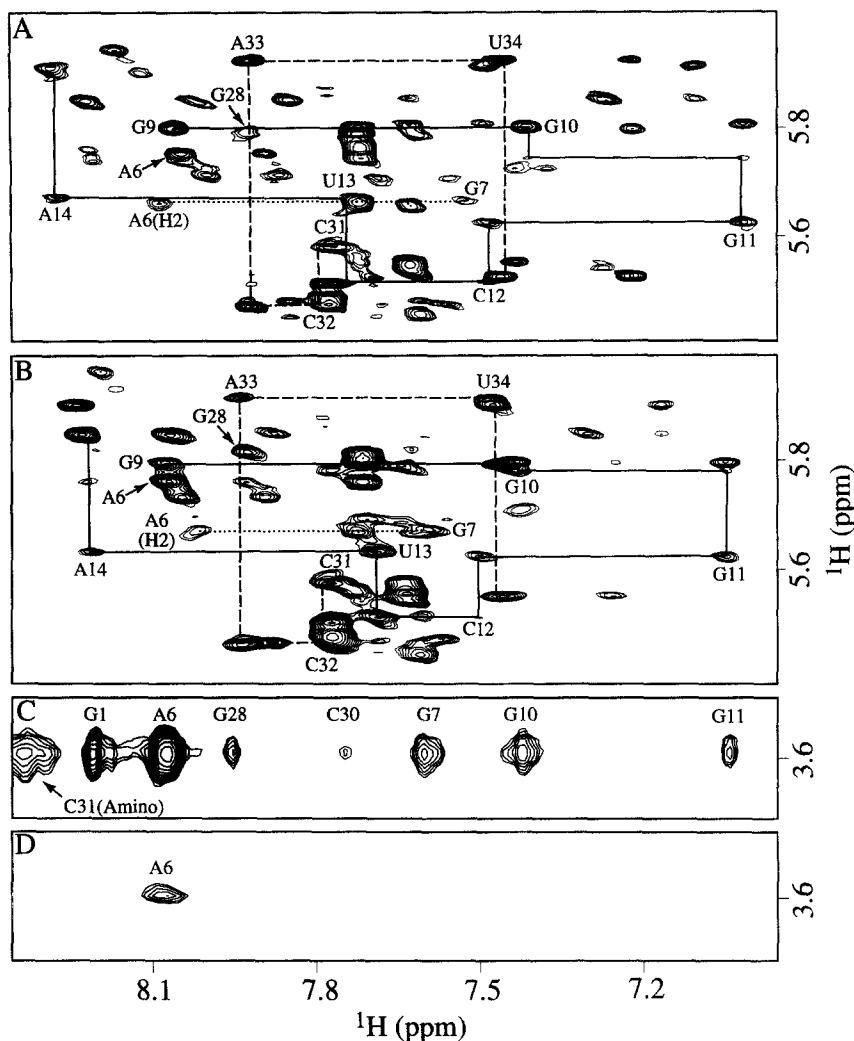


FIG. 4. Aromatic to H1' region of a 400 ms D<sub>2</sub>O NOESY of the VPK pseudoknot in the presence of (A) 5 mM Mg<sup>2+</sup> or (B) 2 mM Co(NH<sub>3</sub>)<sub>6</sub><sup>3+</sup>. The continuous and broken lines indicate standard A-form walks for the two strands of stem 2. The dotted line indicates the A6H2 to G7H8 connectivity that is observed in loop 1. Arrows denote the A6 and G7 intranucleotide H8 to H1' NOE. (C) The Co(NH<sub>3</sub>)<sub>6</sub><sup>3+</sup> proton to H6/H8 region of a 300 ms H<sub>2</sub>O NOESY experiment. Intermolecular NOE cross peaks are observed between Co(NH<sub>3</sub>)<sub>6</sub><sup>3+</sup> protons and the H6/H8 proton of the denoted nucleotide. (D) The Co(NH<sub>3</sub>)<sub>6</sub><sup>3+</sup> proton to H6/H8 region of a <sup>13</sup>C-resolved HSQC-NOESY on a VPK sample selectively <sup>13</sup>C-labeled at the adenine C8 and the uracil C6. Only one cross peak, to the A6H8, is observed. Sample conditions in (A) are 2 mM VPK, 5 mM Mg<sup>2+</sup>, 10 mM sodium phosphate (pH 6.4), 200 mM NaCl, and 100 μM EDTA at a temperature of 30°. Sample conditions in (B), (C), and (D) are identical, with the exception of 2 mM Co(NH<sub>3</sub>)<sub>6</sub><sup>3+</sup> instead of 5 mM Mg<sup>2+</sup>, and a temperature of 35°. [Reprinted with permission from R. L. Gonzalez, Jr. and I. Tinoco, Jr., *J. Mol. Biol.* **289**, 1267 (1999).]

to detect because of severe overlap of the sugar region and close proximity to the suppressed water resonance.

One important difference between  $\text{Mg}(\text{H}_2\text{O})_6^{2+}$  and  $\text{Co}(\text{NH}_3)_6^{3+}$  is that  $\text{Mg}(\text{H}_2\text{O})_6^{2+}$  can give up  $\text{H}_2\text{O}$  ligands and form direct inner-sphere coordinate bonds to RNA. Clearly, when direct coordinate bonds between the metal ion center and RNA functional groups are present,  $\text{Co}(\text{NH}_3)_6^{3+}$  will not be a good mimic for the interaction.

There are several ways to test if  $\text{Co}(\text{NH}_3)_6^{3+}$  is a valid substitute for a metal ion binding site. Two transitions in the ultraviolet absorbance melting curves of the VPK pseudoknot in sodium ion displayed very similar stabilization effects as a function of  $\text{Co}(\text{NH}_3)_6^{3+}$  and of  $\text{Mg}(\text{H}_2\text{O})_6^{2+}$  concentration. Additionally, both  $\text{Co}(\text{NH}_3)_6^{3+}$  and  $\text{Mg}(\text{H}_2\text{O})_6^{2+}$  had similar effects on the VPK imino proton chemical shifts. Furthermore,  $\text{D}_2\text{O}$  NOESYs recorded in the presence of  $\text{Mg}(\text{H}_2\text{O})_6^{2+}$  or  $\text{Co}(\text{NH}_3)_6^{3+}$  exhibit analogous NOE connectivities and intensities, thus indicating that the RNA structure in  $\text{Mg}^{2+}$  is analogous to the structure in  $\text{Co}(\text{NH}_3)_6^{3+}$  (Figs. 4A and 4B). These results corroborate the role of  $\text{Co}(\text{NH}_3)_6^{3+}$  as a probe of the  $\text{Mg}^{2+}$  binding site and indicate that the hexahydrated magnesium ion complex is the form of magnesium ion interacting with the VPK pseudoknot. In cases of direct coordination of the metal ion, a more appropriate probe can be used. For example, in order to mimic a metal ion binding site involving a pentahydrated magnesium ion with one direct coordinate bond to RNA,  $\text{Co}(\text{NH}_3)_5^{3+}$  could be used as a mimic of  $\text{Mg}(\text{H}_2\text{O})_5^{2+}$  where both metal ion complexes can give up one  $\text{H}_2\text{O}$  ligand and form a direct coordinate bond. Similarly, various other complexes of cobalt, or other transition metals, can be used as analogs of directly coordinated magnesium ion complexes.

## Paramagnetic Metal Ion Probes

Unlike titrations utilizing diamagnetic metal ions, titration of an RNA molecule with paramagnetic metal ions can cause relatively large and dramatic NMR spectral changes. As with diamagnetic probes, the RNA sample is titrated with metal ion and one-dimensional experiments are recorded in either 90%  $\text{H}_2\text{O}/10\%$   $\text{D}_2\text{O}$  or 99.9%  $\text{D}_2\text{O}$  solution. The chemical shifts and/or line widths of well-resolved RNA resonances are then recorded as a function of metal ion concentration. Again, the favorable properties of the imino proton region of the spectra provide a good place to begin spectral analysis. The large changes observed in the chemical shifts and/or line widths of the RNA resonances on addition of paramagnetic metal ions are easier to interpret than changes observed during titration with diamagnetic metal ions. This is because the spectral changes observed in the paramagnetic case are dominated by the strong interactions between the unpaired electron spin and nearby ( $\sim 10$  Å) nuclear spins in a distance-dependent manner.<sup>19,22,23</sup> In most cases, small chemical shift or line-width changes associated with minor conformational changes on metal ion binding will be easily separated from the relatively larger

effect of an unpaired electron with a very large magnetic moment in the vicinity of an NMR-active nucleus.<sup>15</sup>

### *Relaxation Rate Enhancement by Paramagnetic Metal Ions*

Perhaps the most widely employed technique for identifying metal ion binding sites in RNA is paramagnetic line broadening. When a paramagnetic ion, such as  $\text{Mn}^{2+}$ , is located within  $\sim 10 \text{ \AA}$  of an NMR-active nucleus, the nucleus will experience an increased rate of relaxation. Enhanced rate of spin-spin ( $T_2$ ) relaxation, in particular, leads to the observation of line broadening in titrations with paramagnetic metal ions.<sup>23</sup> In most cases, the dipolar interaction between the unpaired electron and the nucleus dominates the observed relaxation rate enhancement because of the large electronic magnetic moment. Relaxation rate enhancement due to this dipolar mechanism has an  $r^{-6}$  distance dependence where  $r$  is the distance between the paramagnetic metal ion center and the observed nucleus.<sup>18,19,23-30</sup>

The metal ion in an RNA-metal ion complex is typically weakly bound and has a correspondingly short residence lifetime. Therefore, a single paramagnetic ion can cause enhanced relaxation rates of NMR-active nuclei on multiple sites and multiple RNA molecules. As a result, substoichiometric amounts of  $\text{Mn}^{2+}$  will lead to complete broadening of nuclei in the vicinity of the binding site and at higher concentrations will begin to affect all RNA resonances in a nonspecific manner.

Paramagnetic line broadening of imino proton resonances caused by  $\text{Mn}^{2+}$  has been used to identify metal ion binding sites in tandem G · U wobble base pairs<sup>7</sup> and in the GAAA tetraloop.<sup>5</sup> In both cases the paramagnetic broadening data agree well with the binding site identified through chemical shift changes observed with  $\text{Mg}^{2+}$  or  $\text{Co}(\text{NH}_3)_6^{3+}$  titrations, and with intermolecular NOEs observed from the  $\text{Co}(\text{NH}_3)_6^{3+}$  protons to RNA protons at the binding site. In addition, paramagnetic line broadening by  $\text{Mn}^{2+}$  has been used to identify and localize  $\text{Mg}^{2+}$  binding sites in numerous RNA or RNA-protein complexes,<sup>16,18,19,27,31,32</sup> including the P1 helix from the *T. thermophila* group I intron (Fig. 5).<sup>26</sup> In addition,

<sup>22</sup> R. E. Hurd, E. Azhderian, and B. R. Reid, *Biochemistry* **18**, 4012 (1979).

<sup>23</sup> D. J. Craik and K. A. Higgins, *Ann. Rep. NMR Spectr.* **22**, 61 (1989).

<sup>24</sup> I. Solomon, *Phys. Rev.* **99**, 559 (1959).

<sup>25</sup> N. Bloembergen, *J. Chem. Phys.* **27**, 572 (1957).

<sup>26</sup> F. H.-T. Allain and G. Varani, *Nucl. Acids Res.* **23**, 341 (1995).

<sup>27</sup> B. L. Bean, R. Koren, and A. S. Mildvan, *Biochemistry* **16**, 3322 (1977).

<sup>28</sup> D. Bentrop, I. Bertini, M. A. Cremonini, S. Fors en, C. Luchinat, and A. Malmendal, *Biochemistry* **36**, 11605 (1997).

<sup>29</sup> K. Tu and M. Gochin, *J. Am. Chem. Soc.* **121**, 9276 (1999).

<sup>30</sup> M. Gochin, *Structure* **8**, 441 (2000).

<sup>31</sup> P. F. Agris and S. C. Brown, *Methods Enzymol.* **261**, 270 (1995).

<sup>32</sup> D. G. Gorenstein, E. M. Goldfield, R. Chen, K. Kovarand, and B. A. Luxon, *Biochemistry* **20**, 2141 (1981).

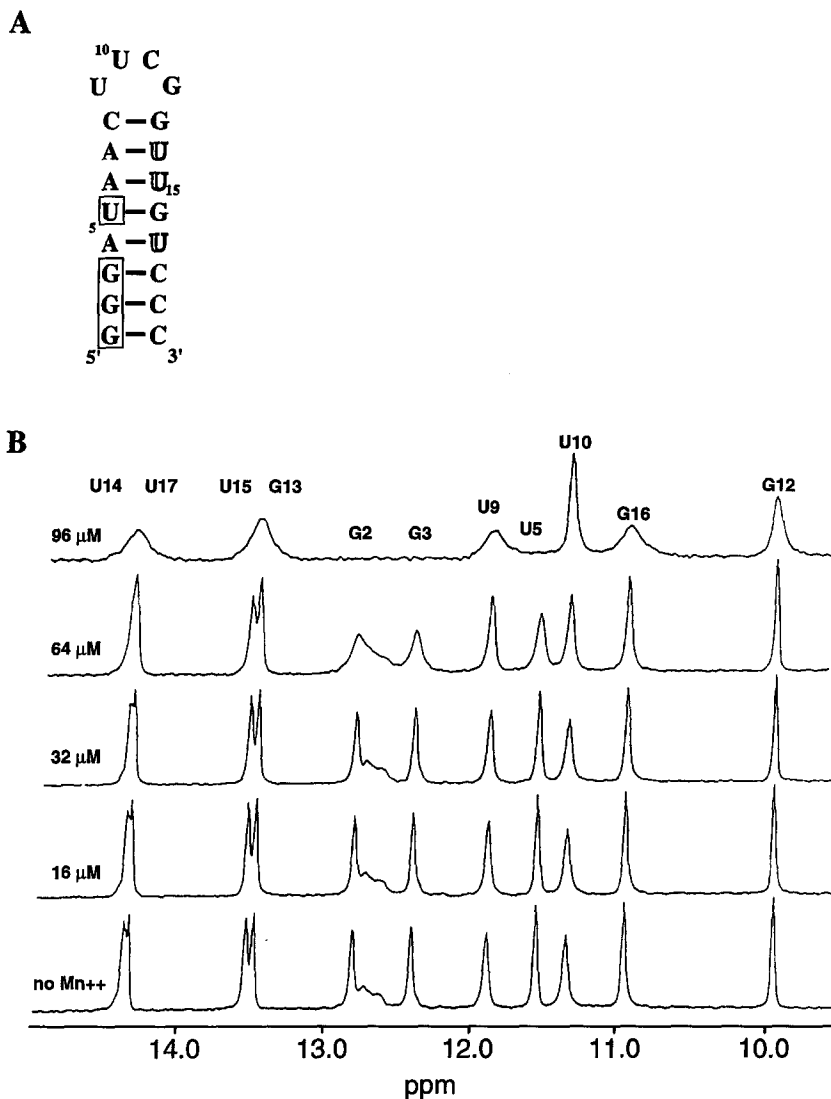
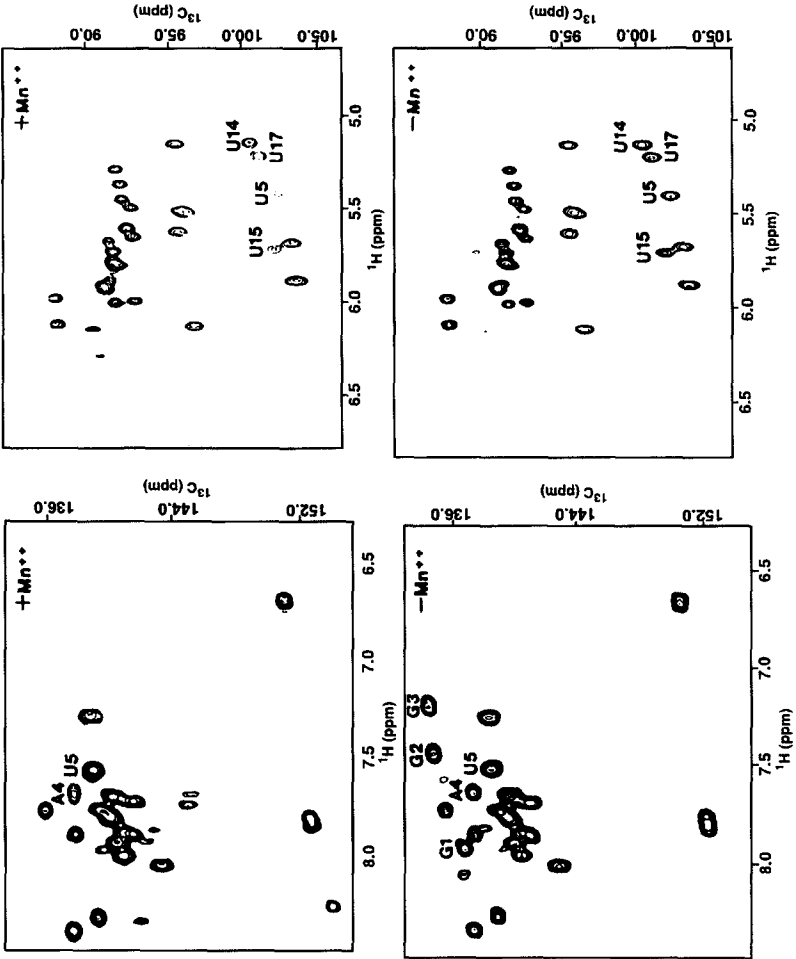


FIG. 5. (A) Sequence and secondary structure of the P1 helix from the *T. thermophila* group I intron. Nucleotides with strongly broadened imino protons by  $\text{Mn}^{2+}$  are boxed and those with slightly broadened imino protons are shown in outline form. (B)  $\text{Mn}^{2+}$  titration of the P1 helix from 1D spectra acquired in  $\text{H}_2\text{O}$  at 275 K at increasing concentrations of  $\text{Mn}^{2+}$ , as indicated next to each spectrum. Assignments are indicated at the top of the figure. (Reprinted from Ref. 40.) (C) Comparison of the  $^1\text{H}$ - $^{13}\text{C}$  correlated (HSQC) spectra of the P1 helix in the presence (top) and absence (bottom) of manganese impurities. The region shown on the right-hand side contains correlations between base resonances (H2, H8, and H6) and their attached carbons. The region on the left-hand side contains correlations between pyrimidine H5 and all H1' resonances and their attached carbons. [Reprinted with permission from F. H.-T. Allain and G. Varani, *Nucl. Acids Res.* **23**, 341 (1995).]



C

paramagnetic  $\text{Ni}^{2+}$  has been used to identify a  $\text{Ni}^{2+}$  ion binding site in an *in vitro* selected  $\text{Ni}^{2+}$  binding RNA aptamer.<sup>33</sup>

In a typical experiment,<sup>26</sup> a one-dimensional experiment in 90%  $\text{H}_2\text{O}/10\% \text{D}_2\text{O}$  is recorded using the jump-return water suppression technique on a 1 mM RNA sample in the absence of divalent metal ions.  $\text{MnCl}_2$  is then added directly to the sample in small increments (of approximately 10–20  $\mu\text{M}$ ) from a 2 mM  $\text{MnCl}_2$  stock solution to cover a range of 4–200  $\mu\text{M}$   $\text{Mn}^{2+}$  concentration. This allows analysis of the imino proton region of the RNA spectrum (Fig. 5B). The titration can also be performed using a one-dimensional experiment or two-dimensional COSY, TOCSY, or NOESY type experiments in 99.9%  $\text{D}_2\text{O}$  with a presaturation pulse during the relaxation delay to suppress the residual HDO peak, in order to observe effects on nonexchangeable protons. Natural abundance  $^1\text{H}$ – $^{13}\text{C}$  or, in an isotopically labeled RNA molecule,  $^1\text{H}$ – $^{15}\text{N}$  or  $^1\text{H}$ – $^{13}\text{C}$  HSQC<sup>19,26</sup> or HMQC experiments can be used to observe line broadening of  $^1\text{H}$  and  $^{13}\text{C}$  or  $^{15}\text{N}$  (Fig. 5C).  $^{31}\text{P}$  line broadening can be observed in one-dimensional phosphorus experiments<sup>18</sup> for unusually well resolved  $^{31}\text{P}$  resonances, or two-dimensional  $^1\text{H}$ – $^{31}\text{P}$  COSY experiments can be used to measure  $^1\text{H}$  and  $^{31}\text{P}$  line broadening for less well resolved  $^{31}\text{P}$  resonances.

#### *Contact and Dipolar (Pseudocontact) Shifts by Paramagnetic Metal Ions*

The chemical shift changes and relaxation rate enhancements observed for magnetic nuclei in the vicinity of paramagnetic metal ions are due to two types of interactions between the unpaired electron spin and the nuclear spin. The first of these, the Fermi contact interaction, is a through-bond, scalar interaction that involves the direct transfer of unpaired electron spin density to the nuclear spin.<sup>23,34,35</sup> Although the contact interaction is useful in identifying nuclei near the paramagnetic metal ion, no quantitative distance information can be derived from the magnitude of the interaction.

The second type of interaction between an unpaired electron spin and a nuclear spin is a through-space dipolar interaction also known as the pseudocontact interaction. Chemical shift changes caused by this mechanism are called pseudocontact shifts and depend primarily on two factors: the angular dependence of the magnetic susceptibility tensor centered on the paramagnetic metal ion center, and a long-range,  $r^{-3}$  distance dependence where  $r$  is the distance between the paramagnetic metal ion center and the nucleus. Pseudocontact shifts have been measured in cytochromes where chemical shifts are measured for the diamagnetic, reduced

<sup>33</sup> H.-P. Hoffman, S. Limmer, V. Hornung, and M. Sprinzl, *RNA* **3**, 1289 (1997).

<sup>34</sup> M. Gochin and H. Roder, *Protein Sci.* **4**, 296 (1995).

<sup>35</sup> M. Gochin and H. Roder, *Bull. Magn. Reson.* **17**, 1 (1995).

[Fe(II)] heme state and for the paramagnetic, oxidized [Fe(III)] heme state.<sup>34–38</sup> Pseudocontact shifts have also been measured in the N-terminal domain of calmodulin where chemical shifts in the diamagnetic reference state were measured for the  $\text{Ca}^{2+}$ -bound form and the chemical shifts in the paramagnetic state were measured by replacing the  $\text{Ca}^{2+}$  ions with paramagnetic  $\text{Ce}^{2+}$  ions.<sup>28</sup> Most recently, pseudocontact shifts have been measured in a DNA–chromomycin–Co(II) complex.<sup>29,30</sup> To make use of the measured pseudocontact shifts, the relationship between the magnetic susceptibility tensor centered on the paramagnetic ion and the molecular coordinate frame must be known.<sup>28–30,34–38</sup>

Although pseudocontact shifts from paramagnetic metal ions have not yet been applied to structural determination of RNA metal ion binding sites, their use clearly seems advantageous. The distance constraints derived from the shifts would be useful not only in very accurately locating the metal ion, but also in providing long-range distance constraints that would better define global features of the RNA structure. In fact, work on the structure of a DNA–chromomycin–Co(II) complex refined against pseudocontact shifts has provided a structure determined to 0.7 Å resolution.<sup>29,30</sup> Global features and fine details of this structure, including differences in the precise location of the drug, are defined to much higher precision in this structure compared to previous NMR structural studies of this complex.<sup>29,30</sup> Co(II),<sup>39–41</sup> Ni(II),<sup>42</sup> Fe(II),<sup>37,38</sup> and the lanthanide(III) metal ions [except for Gd(III)]<sup>28</sup> are all paramagnetic metal ions with asymmetric magnetic susceptibility tensors and fast electron spin relaxation; they are ideal for measurement of pseudocontact shifts.  $\text{Tb}^{3+}$  has been shown to block activity of a hammerhead ribozyme by substituting one catalytically important  $\text{Mg}^{2+}$  ion,<sup>43</sup> and both  $\text{Tb}^{3+}$  and  $\text{Eu}^{3+}$  have been used in luminescence spectroscopy studies of metal ion binding sites in the hammerhead ribozyme.<sup>44</sup> These results demonstrate that substitution of  $\text{Mg}^{2+}$  by lanthanide(III) ions in RNA is possible and perhaps could be used to measure pseudocontact shifts. Studies are currently underway to

<sup>36</sup> R. D. Guiles, S. Sarma, R. J. Digate, D. Banville, V. J. Basus, I. D. Kuntz, and L. Waskell, *Nature Struct. Biol.* **3**, 333 (1996).

<sup>37</sup> L. Banci, I. Bertini, H. B. Gray, C. Luchinat, T. Reddig, A. Rosato, and P. Turano, *Biochemistry* **36**, 9867 (1997).

<sup>38</sup> L. Banci, I. Bertini, K. L. Bren, H. B. Gray, P. Sompornpisut, and P. Turano, *Biochemistry* **36**, 8992 (1997).

<sup>39</sup> I. Bertini, L. Banci, and C. Luchinat, *Methods Enzymol.* **177**, 246 (1989).

<sup>40</sup> I. Bertini, C. Luchinat, and M. Piccioli, *Prog. Nucl. Magn. Reson. Spectrosc.* **26**, 91 (1994).

<sup>41</sup> J. M. Mortal, J. Salgado, A. Donaire, H. R. Jiménez, and J. Castells, *Inorg. Chem.* **32**, 3578 (1993).

<sup>42</sup> J. M. Mortal, J. Salgado, A. Donaire, H. R. Jiménez, and J. Castells, *J. Chem. Soc., Chem. Commun.* **110**, (1993).

<sup>43</sup> A. L. Feig, W. G. Scott, and O. C. Uhlenbeck, *Science* **279**, 81 (1998).

<sup>44</sup> A. L. Feig, M. Panek, W. D. Horrocks, and O. C. Uhlenbeck, *Chem. Biol.* **6**, 801 (1999).

use  $\text{Yb}^{3+}$  to substitute  $\text{Mg}^{2+}$  binding sites in order to measure pseudocontact shifts in various RNA molecules (G. Pintacuda, personal communication, 2000).

### NMR-Active Metal Ion Probes

The direct observation of NMR-active metal ions such as  $^{199}\text{Hg}^{45,46}$  and  $^{113}\text{Cd}^{46,47}$  has provided much information about metal ion binding sites in proteins.  $^{59}\text{Co}$  NMR and  $^{23}\text{Na}$  have been used to study  $\text{Co}(\text{NH}_3)_6^{3+}$  and  $\text{Na}^+$  binding to B-DNA,<sup>48</sup> and  $^{113}\text{Cd}$  has been used to study a metal ion binding site in a small ribozyme.<sup>49</sup> Direct NMR spectroscopy of the metal ion provides unique information from analysis of NMR parameters such as chemical shifts, scalar couplings, and resonance line widths in one-dimensional experiments. It is possible to record spectra with reasonable signal-to-noise on 0.5 ml of a 96% isotopically enriched  $^{113}\text{Cd}$  sample at a concentration of 1–5 mM in a 5 mm NMR tube and a field strength of 11.5 T (500 MHz for  $^1\text{H}$ ).<sup>47</sup> Similarly, a 91% isotopically enriched, 0.4 ml sample of 1–2 mM  $^{199}\text{Hg}$  in a 5 mm NMR tube at a field strength of 14.09 T (600 MHz for  $^1\text{H}$ ) is adequate to detect  $^{199}\text{Hg}$  with a reasonable signal-to-noise ratio.<sup>45</sup>

### Chemical Shift

The NMR spectrum of an NMR-active metal nucleus is very simple, as only one resonance is observed for each metal ion bound. In most cases, the chemical shift range of the metal ion is very large. For example,  $^{113}\text{Cd}$  has a chemical shift range of 800–900 ppm<sup>47</sup> and  $^{199}\text{Hg}$  has a chemical shift range of more than 5000 ppm.<sup>45</sup> Because of these very large chemical shift ranges, the chemical shift of an NMR-active metal nucleus is exquisitely sensitive to the complexation state of the ion.<sup>49,50</sup> The chemical shift can be used to determine the number of ligands,<sup>45</sup> identity of the ligand donor atoms,<sup>45,47</sup> and the complexation geometry in some cases.<sup>45</sup> Currently, such information about metal ion binding sites in RNA is generally only available from crystallographic studies. A  $^{113}\text{Cd}$  NMR study of a small ribozyme revealed a 9 ppm chemical shift change and a 40 Hz increase in line width in the single  $^{113}\text{Cd}$  resonance upon addition of the ribozyme. This effect on the  $^{113}\text{Cd}$  chemical shift and line width indicated specific binding of the metal ion by the RNA, but no details of the interactions were elucidated.<sup>49</sup>

<sup>45</sup> L. M. Utschig, J. W. Bryson, and T. V. O'Halloran, *Science* **268**, 380 (1995).

<sup>46</sup> P. R. Blake, B. Lee, M. F. Summers, M. W. W. Adams, J.-B. Park, Z. H. Zhou, and A. Bax, *J. Biomolec. NMR* **2**, 527 (1992).

<sup>47</sup> J. E. Coleman, *Methods Enzymol.* **227**, 16 (1993).

<sup>48</sup> W. H. Braunlin, C. F. Anderson, and M. T. Record, Jr., *Biochemistry* **26**, 7724 (1987).

<sup>49</sup> M. Vogtherr and S. Limmer, *FEBS Lett.* **433**, 301 (1998).

<sup>50</sup> R. J. Goodfellow, in "Multinuclear NMR" (J. Mason, ed.), p. 563. Plenum Press, New York, 1987.

### Scalar Coupling

In proteins, scalar coupling has been observed between  $^{199}\text{Hg}$  or  $^{113}\text{Cd}$  metal ions and  $^1\text{H}$ ,  $^{13}\text{C}$ ,  $^{15}\text{N}$ , or  $^{31}\text{P}$  resonances in the protein in cases of direct coordination of the metal ion.<sup>45–47</sup> These scalar couplings can be observed indirectly by comparing cross-peak patterns in  $^1\text{H}$ – $^1\text{H}$  COSY or  $^1\text{H}$ – $^{13}\text{C}/^{15}\text{N}$  HMQC experiments recorded in the presence of a spin-0 metal ion and in the presence of a spin-1/2 ( $^{199}\text{Hg}$  or  $^{113}\text{Cd}$ ) metal ion without decoupling of the metal ion. Scalar couplings can also be detected and their values measured directly by analyzing fine structure in the one-dimensional  $^{113}\text{Cd}$  or  $^{199}\text{Hg}$  spectrum<sup>47</sup> or by recording  $^1\text{H}$ – $^{199}\text{Hg}$  or  $^1\text{H}$ – $^{113}\text{Cd}$  HMQC experiments.<sup>45,47</sup> Observation of scalar coupling can provide much structural data about the metal ion binding site. It can help identify which atoms on which side chains are directly coordinated to the metal ion, information that sometimes cannot be unambiguously determined by X-ray crystallographic analysis. In addition, two-bond scalar coupling values can potentially provide information about bond angles, and three-bond scalar coupling values will vary in a Karplus fashion and provide dihedral angle information. Further development of these methods for studying RNA–metal ion interactions should provide new and unique structural information.

### Structure Determination of Metal Ion Binding Sites in RNA

Distance and/or angular constraints generated from intermolecular NOEs, paramagnetic  $T_2$  relaxation rate enhancements, or paramagnetic pseudocontact shifts can be used in a structure calculation protocol in order to solve the structure of the metal ion binding site. Intermolecular NOEs between  $\text{Co}(\text{NH}_3)_6^{3+}$  protons and RNA protons have been used to solve the structures of four metal ion binding sites in RNA.<sup>5–8</sup> If the metal ion complex is observed to sample all possible orientations within the binding pocket, the metal atom can be used as a pseudoatom for the entire metal ion complex with a correction to the intermolecular distance to account for the radius of the ion complex [2.5 Å for  $\text{Co}(\text{NH}_3)_6^{3+}$ ].<sup>6,51,52</sup> Direct coordination of the metal ion complex will exhibit a preferred orientation within the binding pocket, and intermolecular distances can be referenced to a unique proton type in the metal ion complex. NOEs from the  $\text{Co}(\text{NH}_3)_6^{3+}$  protons to RNA imino and amino protons are assigned conservative distance constraints of 0–5 Å (not including the 2.5 Å ionic radius) due to the nonuniform excitation profile of the jump-return water suppression technique and chemical exchange of the protons with solvent. Since the  $\text{Co}(\text{NH}_3)_6^{3+}$  protons exchange slowly on the time scale of

<sup>51</sup> G. J. Kruger and E. C. Reynhardt, *Acta Crystallogr.* **34**, 915 (1978).

<sup>52</sup> J. S. Kieft, "Structure and Thermodynamics of a Metal Ion Binding Site in the RNA Major Groove: Cobalt(III) Hexammine as a Probe." Ph.D. Thesis, University of California, Berkeley, 1997.

one  $t_1$  acquisition block during the NMR experiment,<sup>53</sup> these can be essentially treated as nonexchangeable. Therefore, intermolecular NOEs to nonexchangeable RNA protons can be categorized into strong, medium, and weak categories based on NOE cross-peak intensities. There are two general methods for carrying out the structure calculation as outlined below.

#### *Docking of Metal Ion onto Static NMR Structure*

In this approach the structure of the RNA molecule is determined initially using well-established structure calculation protocols.<sup>54,55</sup> The lowest energy structure or the average structure can then be used to dock the metal ion complex. The RNA coordinates are held static throughout the rest of the calculation and the metal ion complex is docked using the experimentally determined intermolecular distance restraints. There are several structure calculation programs available to do the docking. Both Discover 3<sup>6,52</sup> (Molecular Simulations, Inc., San Diego, CA) and XPLOR<sup>7</sup> scripts have been utilized to dock  $\text{Co}(\text{NH}_3)_6^{3+}$  to two RNA hairpins containing tandem G · U wobble base pairs. The protocol in both cases is similar. The  $\text{Co}(\text{NH}_3)_6^{3+}$  metal ion coordinates are generated using the Builder Module within InsightII (Molecular Simulations, Inc.). The bond lengths and bond angles can be adjusted by energy minimization with Discover 3 (Molecular Simulations, Inc.) using the extensible systematic force field (ESFF). Coordinates derived in this manner are consistent with the published crystal structure of  $\text{Co}(\text{NH}_3)_6^{3+}$ .<sup>6,51,52</sup> Alternatively, the equilibrium bond lengths and bond angles can be taken directly from the published crystal structure<sup>51</sup> and input into X-PLOR.<sup>7</sup> The Lennard–Jones terms and atomic partial charges in both cases are derived from the ESFF forcefield. The  $\text{Co}(\text{NH}_3)_6^{3+}$  metal ion complex is placed in a random translational and rotational position relative to the RNA molecule, and intermolecular distance constraints are then applied during an energy minimization protocol in Discover 3<sup>6,51</sup> or a restrained molecular dynamics protocol using XPLOR<sup>7</sup> until the intermolecular distance constraints are satisfied without the Lennard–Jones or electrostatics force field terms turned on. In a second stage an energy minimization is carried out using the previous constraints, as well as full Lennard–Jones and electrostatic force field terms in order to find the lowest energy orientation(s) of the  $\text{Co}(\text{NH}_3)_6^{3+}$  metal ion complex within the binding pocket. This procedure is repeated with random initial positioning of the  $\text{Co}(\text{NH}_3)_6^{3+}$  ion in order to obtain a family of structures displaying the metal ion binding site. The final structures can be analyzed to determine the RMSD of the metal ion complex within the binding

<sup>53</sup> J. S. Anderson, H. V. A. Briscoe, and N. L. Spoor, *J. Chem. Soc.*, 361 (1943).

<sup>54</sup> B. T. Wimberley, "NMR Derived Structures of RNA Loops: The Conformation of Eukaryotic 5S Ribosomal Loop E." Ph.D. Thesis, University of California, Berkeley, 1992.

<sup>55</sup> G. Varani, F. Aboul-ela, and F. H.-T. Allain, *Prog. Nucl. Magn. Reson. Spect.* **29**, 51 (1996).

pocket as well as to determine the range of possible orientations of the metal ion complex that are consistent with the NMR data.

### *Complete Structure Calculation Including Metal Ions*

A different approach was used in solving the structure of the metal ion binding sites in the VPK frameshifting viral RNA pseudoknot<sup>8</sup> and the GAAA tetraloop<sup>5</sup> in which the metal ion complex was included in all stages of the structure calculations and was used as a structural constraint in itself by not holding the RNA coordinates static at any time during the calculation. Starting structures with random torsion angles were generated, including random positioning of a  $\text{Co}(\text{NH}_3)_6^{3+}$  ion complex. Loose intermolecular distance constraints of 0–10 Å (not including the pseudoatom correction) were used during the global fold stage<sup>54,55</sup> of the VPK pseudoknot structure calculation. During the refinement stage<sup>54,55</sup> of the structure calculation, intermolecular distance constraints were tightened to 0–5 Å (not including the pseudoatom correction) for distance constraints involving exchangeable RNA protons, and categories of strong, medium, and weak for distance constraints involving nonexchangeable RNA protons. In the final energy minimization stage,<sup>54,55</sup> full Lennard–Jones and electrostatic potential force field terms were turned on. In the GAAA tetraloop structure calculation, the same intermolecular distance ranges were used in the global fold, refinement, and minimization stages.  $\text{Co}(\text{NH}_3)_6^{3+}$  proton to RNA exchangeable proton cross peaks were put into a loose 1.8–5.0 Å (without pseudoatom correction) category. Intermolecular cross peaks involving nonexchangeable RNA cross peaks were categorized as strong, medium, weak, or very weak. The rest of the structure calculation was carried out in a manner analogous to that for the VPK pseudoknot. This approach was particularly important in the VPK pseudoknot structure calculation where intermolecular NOEs were observed between the  $\text{Co}(\text{NH}_3)_6^{3+}$  and RNA protons located in stem 2 of and loop 1—a unique tertiary structural feature—of the pseudoknot. The short two-nucleotide loop 1 crosses the major groove face of stem 2 and could certainly impede docking of the metal ion complex if the RNA coordinates were held static. In addition, this provided indirect loop-to-stem connectivities, connectivities that previously have not been observed for this pseudoknot and clearly would be important in determining the structural relationship between loop 1 and stem 2. In fact, previous work on the VPK pseudoknot had required the use of additional, nonexperimental, long-range constraints to prevent the starting structures from forming knotted structures during the initial global folding stage of structure calculation. The inclusion of the  $\text{Co}(\text{NH}_3)_6^{3+}$  metal ion during the global fold eliminated the need for these constraints.<sup>8,56</sup>

<sup>56</sup> L. X. Shen and I. Tinoco, Jr., *J. Mol. Biol.* **247**, 963 (1995).

## Thermodynamic and Kinetic Characterization of Metal Ion Binding Sites

An RNA nucleus in close proximity of a metal ion binding site, or in the vicinity of a metal-induced conformational change, will experience two unique chemical environments. The analogous situation exists for a metal ligand resonance. Analysis of the chemical exchange properties between the metal-free and metal-bound forms of the RNA-metal ion complex can provide thermodynamic and kinetic information about the interaction between the metal ions and the RNA molecule. In this way, NMR provides a unique opportunity to study the kinetics and thermodynamics of the interaction, as well as determine the structure of the RNA-metal ion complex. Diamagnetic or NMR-active metal ion probes are the most useful for thermodynamic and kinetic characterization since the weak binding and the fast exchange condition typical of RNA-metal ion complexes mean that even trace amounts of paramagnetic ions will affect many RNA sites on many RNA molecules.<sup>18</sup> The methods used to obtain thermodynamic and kinetic parameters depend on whether the kinetics of binding are in fast, slow, or intermediate exchange. The following discussion will consist of chemical exchange on the chemical shift time scale, since chemical exchange on the scalar coupling and relaxation rate time scales is generally found in the fast exchange regime and are therefore measured as averages. The fast exchange regime occurs when the rate of exchange between the bound and free states is significantly faster (a factor of 5) than the difference between chemical shifts (in hertz) of the bound and free states. Resonances in the fast exchange regime will display a single resonance at a chemical shift determined by the population weighted average of the individual chemical shifts of the bound and free states. The slow exchange regime occurs when the rate of exchange between the bound and free state is significantly slower (a factor of 1/5) than the difference between the chemical shift of the bound and free states. Resonances in the slow exchange regime will display two distinct resonances at the characteristic chemical shift of the bound and free states with areas proportional to the population of each state. Intermediate exchange occurs when the rate of exchange is approximately equal to the difference in chemical shifts between the bound and free states. Resonances in intermediate exchange will exhibit complicated spectral behavior between that observed in the fast and slow exchange cases.<sup>57</sup>

The most general way to obtain thermodynamic and kinetic information of a chemical exchange process, including metal ion binding to RNA, is line-shape analysis. Line-shape analysis is covered in detail in several reviews.<sup>23,57,58</sup> This technique involves the fitting of computer-simulated line shapes to experimental

<sup>57</sup> L.-Y. Lian and G. C. K. Roberts, in "NMR of Macromolecules: A Practical Approach" (G. C. K. Roberts, ed.), p. 153. Oxford University Press, New York, 1993.

<sup>58</sup> H. S. Gutowsky and C. H. Holm, *J. Chem. Phys.* **25**, 1228 (1956).

line shapes. In general, the imaginary component of the McConnell-modified Bloch equations<sup>59</sup> is used to simulate line shapes for a two-site exchange process in the absence of scalar coupling. These line shapes depend on the population, resonance frequency,  $T_2$  relaxation rate, and exchange lifetime of the metal free and metal bound states. Usually the resonance frequencies and the  $T_2$  relaxation rates for the two states can be experimentally measured or estimated, and the populations and exchange lifetime can then be fitted to the observed line shape using a nonlinear regression program.

Line-shape analysis of RNA (or metal ion) resonances can be done as a function of increasing metal ion (or RNA) concentration. Assuming that a particular resonance is affected by a single metal ion binding at this site, line-shape analysis can provide the on-rate ( $k_{\text{on}}$ ) and off-rate ( $k_{\text{off}}$ ) of metal ion binding, as well as the corresponding equilibrium dissociation constant ( $K_d$ ) at a given temperature. The fast and slow exchange regimes allow a number of simplifications to line-shape analysis, and thermodynamic and kinetic measurements are straightforward in these two extremes.

#### *Thermodynamic and Kinetic Analysis in Fast Exchange Case*

When metal ion binding to RNA is relatively weak ( $K_d \approx 10^{-3} M$ ), the exchange rate is usually in the fast exchange limit. An RNA (or metal ion) resonance that undergoes a change in chemical shift, with no accompanying change in intensity or line width, is in the fast exchange limit.

Changes in chemical shift of RNA protons on titration with  $\text{Co}(\text{NH}_3)_6^{3+}$  or  $\text{Mg}(\text{H}_2\text{O})_6^{2+}$  have been used to study four RNA-metal ion complexes.<sup>5-8</sup> In each case, aliquots of a concentrated (1 M) stock solution of  $\text{Co}(\text{NH}_3)_6^{3+}$  or  $\text{Mg}(\text{H}_2\text{O})_6^{2+}$  are added directly to an NMR sample containing the RNA of interest at a known total RNA concentration in the range of 0.2–0.8 mM in 10 mM sodium phosphate (pH 6.4), 200 mM NaCl, 100  $\mu\text{M}$  EDTA dissolved in 90%  $\text{H}_2\text{O}/10\%$   $\text{D}_2\text{O}$ . A one-dimensional experiment utilizing the jump-return method of water suppression is done at each metal ion concentration and the chemical shift and line width of each imino proton resonance are recorded. The good dispersion of the RNA imino proton spectral region makes it ideal for these titrations. The sample volume change in each titration point is accounted for and the RNA concentration is corrected.

$\text{Co}(\text{NH}_3)_6^{3+}$  or  $\text{Mg}^{2+}$  have been found to be in fast exchange between the free and bound states as well as in fast exchange within the RNA binding pocket in all four RNA- $\text{Co}(\text{NH}_3)_6^{3+}$  complexes studied thus far. During titration of RNA with  $\text{Co}(\text{NH}_3)_6^{3+}$ , all 18  $\text{Co}(\text{NH}_3)_6^{3+}$  protons resonate in a single, broad ( $\sim 15$  Hz) resonance at 3.65 ppm with no significant chemical shift or line-width changes with increasing amounts of  $\text{Co}(\text{NH}_3)_6^{3+}$ . The chemical shift of free  $\text{Co}(\text{NH}_3)_6^{3+}$

<sup>59</sup> H. M. McConnell, *J. Chem. Phys.* **28**, 430 (1958).

protons, with no RNA present, displays similar line width and chemical shift as that of  $\text{Co}(\text{NH}_3)_6^{3+}$  protons in the presence of RNA. The lack of a dramatic chemical shift or line-width change of the  $\text{Co}(\text{NH}_3)_6^{3+}$  proton resonance and the close agreement of these NMR parameters with the same parameters for  $\text{Co}(\text{NH}_3)_6^{3+}$  free in solution is characteristic of a fast exchange process with a large population of free  $\text{Co}(\text{NH}_3)_6^{3+}$  vs bound  $\text{Co}(\text{NH}_3)_6^{3+}$ , or a very small chemical shift difference between the bound and free state of the  $\text{Co}(\text{NH}_3)_6^{3+}$  protons, or a combination of the two.

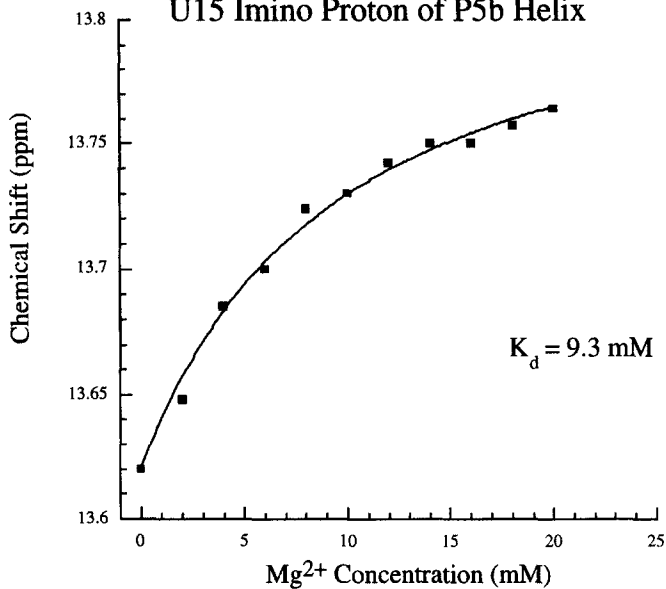
Analysis of RNA imino protons during the titration also indicate fast exchange between bound and free state of the RNA molecule. During the titration, no resonances disappear and no new resonances are observed. Several peaks undergo changes in chemical shift value with no significant changes in line width (Fig. 6). All of this is consistent with a fast exchange process for the binding of the metal ion complex. Some imino protons do display minor amounts of line broadening at higher metal ion concentrations, but this may be due to changes in base pair stability and imino proton exchange with bulk solvent water. Titrations with  $\text{Mg}^{2+}$  or with  $\text{Co}(\text{NH}_3)_6^{3+}$  have similar effects on RNA proton resonances.

In the fast exchange limit, the rate of exchange and the corresponding exchange lifetime cannot be calculated. Calculation of the equilibrium binding constant ( $K_d$ ), however, is very straightforward in the limit of fast exchange. Since there are no changes in line width, the experimental data consist of the chemical shift for the free state (measured in the absence of metal ion) and the observed chemical shift at various increasing concentrations of metal ion. Ideally, the NMR sample is dialyzed against buffer containing the desired metal ion concentration at each titration point. In this way the free metal ion concentration at each titration point is known, and a binding curve of observed chemical shift vs free metal ion concentration can be constructed. A Scatchard plot can provide the number of binding sites and their  $K_d$ . Alternatively, metal ion can be directly added to the NMR sample, and a binding curve of observed chemical shift vs total metal ion concentration can then be plotted (Fig. 6). In favorable cases, the NMR properties of an observed RNA

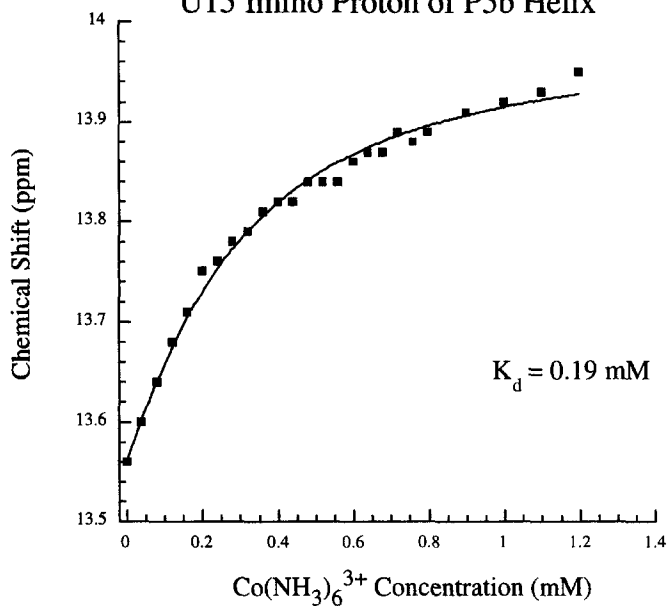
---

FIG. 6. Binding curve of the P5b U15 imino proton vs (A)  $\text{Mg}^{2+}$  or (B)  $\text{Co}(\text{NH}_3)_6^{3+}$  concentration. A change in chemical shift of the U15 imino proton resonance is observed with increasing concentration of (A)  $\text{Mg}^{2+}$  or (B)  $\text{Co}(\text{NH}_3)_6^{3+}$  with no significant change in line width, indicating a fast exchange process on the chemical shift time scale. The equilibrium dissociation constant ( $K_d$ ) for (A)  $\text{Mg}^{2+}$  or (B)  $\text{Co}(\text{NH}_3)_6^{3+}$  binding to the U15 imino proton is calculated by fitting the data to an equation for a one-site binding mode in fast exchange. In (A) and (B) the data are plotted as points and the calculated curve is shown as a solid line. An average  $K_d$  for the metal ion binding site can be determined by performing similar calculations for other RNA protons in the vicinity of the binding site that undergo chemical shift changes as a function of metal ion concentration.

**A** Chemical Shift vs.  $Mg^{2+}$  Concentration  
U15 Imino Proton of P5b Helix



**B** Chemical Shift vs.  $Co(NH_3)_6^{3+}$  Concentration  
U15 Imino Proton of P5b Helix



resonance will be affected chiefly by the direct binding of only one metal ion. The plot of observed chemical shift vs total metal ion concentration can be fitted to an equation for a single metal ion binding site in order to determine  $K_d$  (Fig. 8).<sup>6,8,52,57</sup> This equation has been applied to metal ion titrations in order to determine  $K_d$  for  $\text{Co}(\text{NH}_3)_6^{3+}$  or  $\text{Mg}(\text{H}_2\text{O})_6^{2+}$  in the four metal ion–RNA complexes. In principle, a van't Hoff analysis of the temperature dependence of the binding can provide the enthalpy, entropy, and free energy of binding.

#### *Thermodynamic and Kinetic Analysis in Slow Exchange Case*

Slow exchange on the chemical shift time scale usually occurs in cases of tight binding ( $K_d \approx 10^{-6} M$ )<sup>23</sup> and is not commonly observed in metal ion interactions with RNA. In cases of slow exchange on the chemical shift time scale, individual resonances are observed for the metal free state and the metal bound state. For a well-resolved RNA resonance, the area of each peak will correspond to the population of each state and allow calculation of the free RNA and the RNA–metal ion complex concentrations. Assuming a one metal ion binding site model, the free metal ion concentration and the  $K_d$  can be calculated directly from the population measurements. In cases where both an RNA resonance and a metal ion complex resonance are well resolved, the free RNA, free metal ion, and RNA–metal ion complex concentrations can all be determined from population measurements as a function of metal ion concentration. This again would allow Scatchard analysis of the data. Furthermore, the metal ion concentration dependence of the line widths of the free state resonance from the RNA molecule (or the RNA concentration dependence on a metal ion complex free state resonance) can be used to determine the exchange rates.<sup>57</sup>

#### *Thermodynamic and Kinetic Analysis in Intermediate Exchange Case*

When metal ion binding produces resonances in intermediate exchange,<sup>16</sup> or in slow exchange where only the resonance of one of the two states is well resolved,<sup>18</sup> the simplifications of the fast exchange or the slow exchange limits do not apply and the thermodynamics and kinetics of binding must be determined from a full line-shape analysis.<sup>18,23,57</sup> Line-shape analysis was used to measure the binding affinity of a  $\text{Mg}^{2+}$  ion to the catalytic core of a hammerhead ribozyme<sup>18</sup>—a metal ion that despite its unusually tight binding has not been previously observed by crystallographic or biochemical methods. In this case an unusually well resolved phosphorus resonance was observed to undergo chemical exchange on the chemical shift time scale between the metal bound and the metal free state as a function of increasing  $\text{Mg}^{2+}$  concentration. The chemical shift of the free state was well resolved and was measured in the absence of metal ion. The bound chemical shift, on the other hand, resides in the overcrowded and unresolved region of the RNA phosphorus spectrum. Therefore, several values for the bound state chemical shift

were used, which leads to the uncertainty reported in the measurement. Using the experimentally determined free state chemical shift and a range of bound state chemical shifts, the population and exchange lifetime of the free and bound states were fitted to the experimental data. An equilibrium binding constant of 250–570  $\mu\text{M}$  for the binding of a single  $\text{Mg}^{2+}$  to a specific phosphate group was obtained.

## Conclusion

The interactions of metal ions with RNA are clearly important to RNA structure and function. NMR spectroscopy provides a powerful methodology for the study of these interactions. NMR spectroscopy can provide distance constraints between a metal ion and a binding site in an RNA molecule generated from analysis of paramagnetic relaxation rate enhancements, or intermolecular NOEs. The potential exists for further geometric constraints from pseudocontact shift distance estimates and observation of scalar coupling of RNA atoms to tightly bound, directly coordinated metal ions. In addition to the detailed structural information that is available from NMR spectroscopic techniques, the kinetics and thermodynamics of the interaction can also be determined. Exchange rate constants and equilibrium dissociation constants can be estimated from relatively simple NMR experiments.

## Acknowledgments

This research was supported in part by the National Institutes of Health Grant GM 10840, by the Department of Energy Grant DE-FG03-86ER60406, and through instrumentation grants from the Department of Energy (DE-FG05-86ER75281) and from the National Science Foundation (DMB 86-09305). We thank Ms. Barbara Dengler for managing the laboratory, Mr. David Koh for synthesizing DNA oligonucleotides, and Dr. Jeffrey Pelton for valuable NMR advice.